Effects of potential shift and efficiency of charge collection on nanotube-based porphyrin-sensitized solar cells with conjugated links of varied length†

Liyang Luo,[ab] Chia-Jung Lin,[a] Chen-Shiung Hung,[b] Chen-Fu Lo,[c] Ching-Yao Lin[c] and Eric Wei-Guang Diau*[a]

Received 5th May 2010, Accepted 10th August 2010
DOI: 10.1039/c0cp00458h

For dye-sensitized solar-cell devices fabricated from porphyrin sensitizers with links of varied length (PE1–PE4) adsorbed on anodic titanium-oxide nanotube arrays, we measured induced photocurrent and photovoltage decays under constant bias illumination; the evaluated efficiencies of charge collection of the devices show a systematic trend PE4 > PE3 > PE2 > PE1 at a large short-circuit current, implying that a long link would improve the charge separation if the electrons were effectively injected into the semiconductor.

Dye-sensitized solar cells (DSSC) are prospective photovoltaic devices because they are transparent, flexible, readily processed, economical and environmentally safe.[1] Among efficient sensitizers, porphyrin dyes are particularly attractive because their molecular structures are readily modified to harvest sunlight efficiently from the visible region to the near infrared.[2] A device made of a 'push–pull' zinc porphyrin sensitizer has attained an efficiency of power conversion as great as 11% under one-sun irradiation, stimulating hope that porphyrin dyes might yield highly efficient DSSC applications.[3]

From a mechanistic point of view, electron injection, charge recombination, dye regeneration and electron collection at the electrode are fundamental processes that control the total efficiency (η) of power conversion of a DSSC.[4] Charge separation occurs initially in the dye upon irradiation; electrons subsequently migrate to the interface between the dye and TiO_2 through a bridge or link. To improve the cell performance, careful design of the structure of the dye with an appropriate link can thus minimize the rate of charge recombination.[5] To enhance our understanding of the role of a link with respect to the performance of a porphyrin-based DSSC device, we have designed zinc porphyrins with the length of the link controlled by the number of phenylethynyl (PE) units for a porphyrin, from one PE unit (denoted PE1) up to four PE units (PE4).[6] With PE1–PE4 sensitized on anodic titanium-oxide (ATO) films of one-dimensional nanostructure to make nanotube (NT)-based DSSC devices, the values of η decreased systematically with increasing length of the link.[7] We thus concluded that the aggregate-induced energy transfer is more significant with a long link than a short link to decrease the injected electrons for the observed dependence of the cell performance on length.[7] Because the distance attenuation for the rate coefficient of electron injection of the PE system was small,[7,8] a porphyrin with a long PE link might improve the charge separation, thus increasing the efficiency of charge collection, if the problem of dye aggregation became resolved. In this communication we provide experimental evidence to consolidate the above concept based on an analysis of the kinetics of charge transport obtained from measured photocurrent and photovoltage transients.

We fabricated ordered nanochannel arrays of ATO films at 25 °C on anodizing titanium foil (Aldrich, 99.7%) at a constant voltage 60 V, as reported previously.[9] The ATO films (active size 0.4 × 0.4 cm^2) were then immersed in a THF solution containing PE1–PE4 (1×10^{-4} M) at 40 °C for 3 h to serve as working electrodes; the corresponding absorption spectra of the dye-sensitized films are shown in Fig. S1, ESI.† The fluorine-doped tin oxide (FTO; 30 Ω/sq, Sinonar, Taiwan) glasses (typical size 1.0 × 2.0 cm^2) coated with Pt particles served as counter electrodes, and the corresponding NT-DSSC devices of sandwich type were fabricated according to a procedure reported elsewhere.[7] Current–voltage characteristics were measured with a digital source meter (Keithley 2400) with the devices under AM1.5 one-sun irradiation from a solar simulator (SAN-EI, XES-502S) calibrated with a standard silicon reference cell (VLSI standards, Oriel PN 91150V). Fig. 1 shows the photovoltaic characteristics of the four porphyrin-based DSSC devices fabricated with identical ATO films. Consistent with reported results,[6a,7] the efficiencies of power conversion of these NT-DSSC devices decreased systematically from 3.1% (PE1), 2.5% (PE2), 0.89% (PE3) to 0.22% (PE4). This systematic variation of the cell performance is consistent with the variation of the short-circuit photocurrent density (J_{SC}/mA cm^{-2}), which decreased from 8.3 (PE1), 6.7 (PE2), 2.5 (PE3) to 0.66 (PE4) as the length of the PE link increased accordingly. To acquire an understanding of the observed dependence of performance on the length of the porphyrin-based DSSC, we applied pulsed transients of photocurrent and photovoltage to measure the kinetics of electron transport of the NT-DSSC devices after electron injection from porphyrins.

The experiment to measure the photocurrent decay has been described;[7] the system has been modified (Fig. S2, ESI†) to

[a] *Department of Applied Chemistry and Institute of Molecular Science, National Chiao Tung University, Hsinchu, Taiwan. E-mail: diau@mail.nctu.edu.tw*
[b] *Institute of Chemistry, Academia Sinica, Taipei, Taiwan*
[c] *Department of Applied Chemistry, National Chi Nan University, Puli, Nantou Hsien, Taiwan*

† Electronic supplementary information (ESI) available: Absorption spectra of PE1–PE4 on ATO films; experimental setup for transient photocurrent and photovoltage measurements; photocurrent and photovoltage transients of the NT-DSSC devices formed from PE1–PE4. See DOI: 10.1039/c0cp00458h

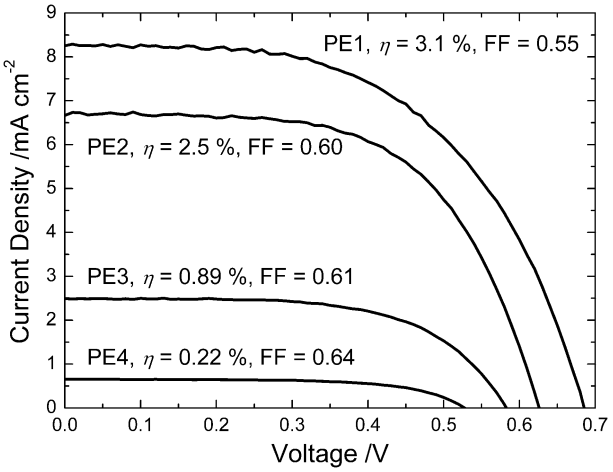

Fig. 1 Current–voltage characteristics of NT-DSSC devices with sensitizers PE1–PE4 collected under one-sun illumination (AM 1.5, 100 mW cm^{-2}).

measure both transient photocurrent and photovoltage decays. The NT-DSSC devices were irradiated from the counter-electrode side with a weak pulse ($\sim$1 μJ $pulse^{-1}$) of light at 430 nm (NT342, EKSPLA, pulse duration $\sim$8 ns) under background (bias) illumination at 632.8 nm. The intensity of the bias light was varied in five steps (photon flux/10^{15} cm^{-2} s^{-1} = 2.2–11) with neutral-density filters. The resulting photocurrent and photovoltage transients were recorded on a digital oscilloscope (LeCroy 9350), with the signals passing a current preamplifier (SR570, SRC) at a short-circuit condition and a voltage preamplifier (SR560, SRC) at an open-circuit condition, respectively. Fig. 2a and b show the typical photocurrent and photovoltage transients, respectively; the raw data and the corresponding analysis of the kinetics of photocurrent transients (Fig. S3–S6†) and photovoltage transients (Fig. S7–S10) of PE1–PE4 devices are reported in the ESI.†

In principle, the large bias illumination provides a constant short-circuit current (I_{SC}) or open-circuit voltage (V_{OC}) at the background level shown in Fig. 2, and the small probe pulse generates a perturbation of the photostationary state for which the relaxation of the transient, either $\Delta I_{SC}(t)$ or $\Delta V_{OC}(t)$, is describable with a suitable kinetic model.[10] For photocurrent decays (Fig. 2a), the transients were fitted with a diffusion equation dependent on time,[7,11]

$$\Delta I_{SC}(t) = \frac{qL\Delta N}{2\sqrt{\pi D t^{3/2}}} \exp\left(-\frac{L^2}{4Dt}\right) \quad (1)$$

in which L (= 15 μm) represents the length of NT arrays; the fitted parameters are the number ΔN and the diffusion coefficient D of the electrons at the short-circuit condition. The collection time coefficient (τ_C) is related to the diffusion coefficient *via* $\tau_C = L^2/(2.35D)$.[10] For photovoltage decays (Fig. 2b), the transients were fitted with a single exponential decay, $\Delta V_{OC}(t) = \Delta V \exp(-t/\tau_R)$, in which fitted parameters are the photovoltage amplitude ΔV and the recombination time coefficient τ_R of the electrons at an open-circuit condition. The chemical capacitance (C) of the TiO_2/porphyrin interface is evaluated as $C = \Delta Q/\Delta V$,[12] in which the injected electron charge ΔQ is determined on integrating the photocurrent transient with time as shown in Fig. 2a.

The chemical capacitance measures the amount of charge that can be stored in trap states of TiO_2; it thereby provides direct information on the density of states (DOS) of the ATO films.[12,13] According to the thermodynamic model of chemical capacitance in nanostructured TiO_2, C is characterized with an exponential dependence on the bias potential.[13] We therefore display C as a function of V_{OC} at five bias intensities for NT-DSSC of PE1–PE4; the corresponding semilogarithmic plots are shown in Fig. 3. The solid lines are simulated results obtained according to the following expression:[13,14]

$$C(V_{OC}) = C_0 \exp\left(\frac{qV_{OC}}{k_B T_0}\right) = C_0 \exp\left(\frac{V_{OC}}{m_C}\right) \quad (2)$$

in which C_0 is the pre-exponential factor, T_0 is a characteristic temperature, and m_C is the characteristic energy describing the curvature of the DOS distribution.[12–14] These plots of C *vs.* V_{OC} of the devices exhibit a systematic trend from PE1 to PE4; *i.e.*, at the same V_{OC} value the order of chemical capacitances is PE4 > PE3 > PE2 $\geq$ PE1.

Because V_{OC} represents the potential difference between the Fermi level of the ATO film and the I^-/I_3^- redox couple of electrolyte,[1,4] and C is proportional to the DOS at that V_{OC},[12] this observation indicates that the DOS of TiO_2 decreases

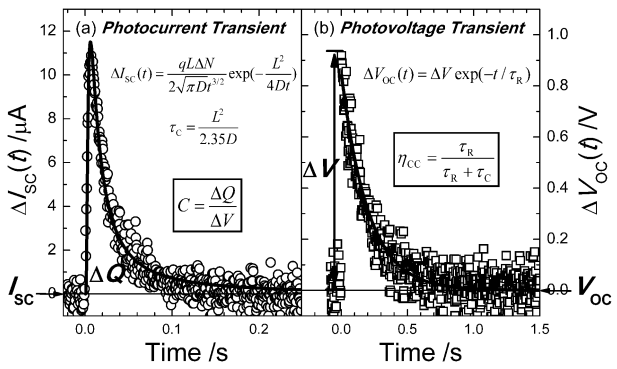

Fig. 2 (a) Photocurrent and (b) photovoltage transients of a typical NT-based porphyrin-sensitized solar cell device characterized with equations and key parameters indicated.

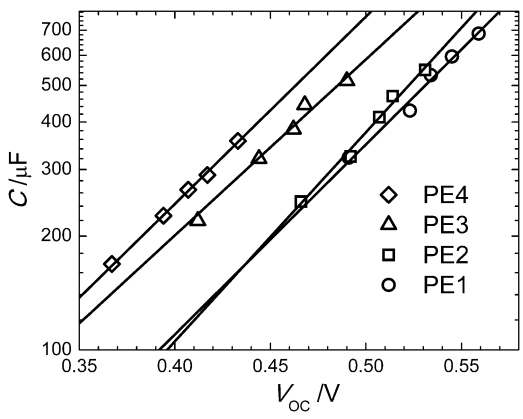

Fig. 3 Semilogarithmic plots of chemical capacitance (C) of NT-DSSC devices of PE1–PE4 as a function of V_{OC}. The solid lines represent exponential fits according to eqn (2).

systematically from PE4 to PE1 at the same Fermi level. The trend of the trap electrons in the conduction band of TiO_2 to reach the same Fermi level for PE1–PE4 must hence result from a systematic band-edge shift of the TiO_2 potential for PE1–PE4;[15] the shift from PE1 to PE4 was observed to be as great as 70 mV. This varied feature of potential shift with dye adsorbed on the TiO_2 surface was also observed on solid-state DSSC, for which a high V_{OC} was related to an upward shift of the TiO_2 conduction band edge toward more negative potentials.[16] The fits of the experimental data according to eqn (2) give m_C/mV = 87 ± 16, 79 ± 13, 93 ± 20 and 88 ± 6 for PE1–PE4, respectively. These results reflect a systematic trend of the steepness of the trap-state distribution of the TiO_2 potentials for PE1–PE4. We conclude that the porphyrin with a long link attached to the surface of ATO results in a slightly broadened TiO_2 potential with a significantly smaller band edge. This conclusion is consistent with the photovoltaic performance of the system (Fig. 1) showing a systematic trend of V_{OC}/mV decreasing from 685 (PE1), 626 (PE2), 583 (PE3) to 528 (PE4).

Mori and co-workers[17] found only a small influence on TiO_2 potential for coumarin dyes with oligothiophene links, and concluded that the smaller V_{OC} for organic DSSC with a long link was due to a smaller electron lifetime resulting from rapid charge recombination. The same conclusion was made for thienylenevinylene oligomers with varied lengths.[18] Moreover, for triphenylpolyene dyes[19] electron recombination is enhanced on increasing the length of the vinylene–thiophene link. The larger dyes were suggested to have a larger polarizability to interact more efficiently with the surrounding species in the electrolyte.[19] In our case, the smaller V_{OC} for the device with a long link was attributed mainly to the factors that fewer electrons were injected into TiO_2 because of dye aggregation,[7] and a downward shift and broadening of the TiO_2 conduction band upon dye uptake (Fig. 3). Fig. 4 shows plots of τ_R *vs.* V_{OC} for PE1–PE4 devices. With a potential shift upwards by 70 mV for PE4 (dashed line in Fig. 4) to match the chemical capacitance of PE1, the durations of charge recombination of PE4 are significantly larger than those of PE1, but the slopes of the plots shown in Fig. 4 vary appreciably: they decreased systematically from PE1 to PE4. Our results might indicate that the dominant recombination was caused by the bulk trapped states for PE3 and PE4, but by the surface-trapped states for PE1 and PE2 in the open-circuit conditions. The PE links in the dye/ATO interface hence affect the depth of distribution of DOS and alter the recombination lifetimes, as we have observed.

The charge collection efficiency (η_{CC}) of a NT-DSSC device is evaluated as $\eta_{CC} = \tau_R/(\tau_C + \tau_R)$,[20] in which τ_C and τ_R were determined from fitting the photocurrent and photovoltage decays demonstrated in Fig. 2a and b, respectively. To relate short-circuit and open-circuit measurements for a given light intensity, one must consider the discrepancy of the charge densities on TiO_2 (or the shift of the Fermi levels) between the two conditions.[21] We predict η_{CC} based on τ_C and τ_R values obtained at the same J_{SC} level so as to correlate the two time coefficients at the same photocharge density. Fig. 5 shows plots of η_{CC} as a function of J_{SC} for PE1–PE4 based on simulated values of τ_C and τ_R; the details are described below.

Both the diffusion correlation time τ_C and the duration of charge recombination τ_R depend strongly on the bias light intensity and are satisfactorily described with a power-law relation with J_{SC},[10,15]

$$\tau_C \text{ or } \tau_R = A(J_{SC})^n \qquad (3)$$

in which A is a pre-exponential factor and n is the exponent of the power dependence. The insets of Fig. 5 show logarithmic plots of the two time coefficients as a function of J_{SC}, fitted according to eqn (3) at five bias light intensities for each porphyrin. For the diffusion time τ_C, n is determined to be −0.64 ± 0.04, −0.67 ± 0.10, −0.73 ± 0.08 and −0.98 ± 0.23 for PE1–PE4, respectively; $(n + 1)$ is related to the steepness of the exponential distribution of trap states, which is inversely proportional to the characteristic energy parameter m_C.[15] The dependence of τ_C *vs.* J_{SC} on power is mild for all porphyrins

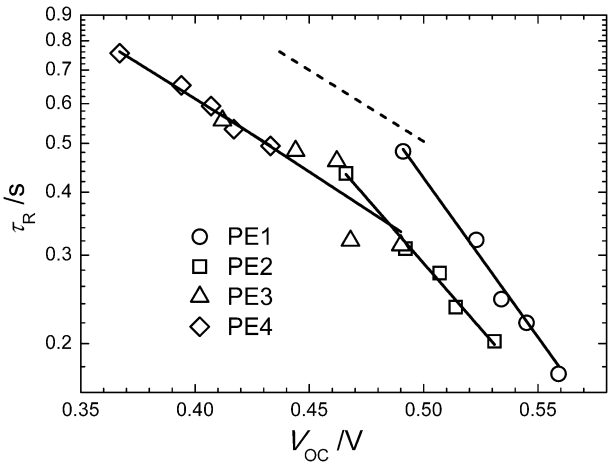

Fig. 4 Semilogarithmic plots of electron lifetime (τ_R) of NT-DSSC devices of PE1–PE4 as a function of V_{OC}. The solid lines represent exponential fits for PE1–PE4. The dashed line shows the fit of PE4 on shifting the potential 70 mV upwards to match the capacitance of PE1 as indicated in Fig. 3.

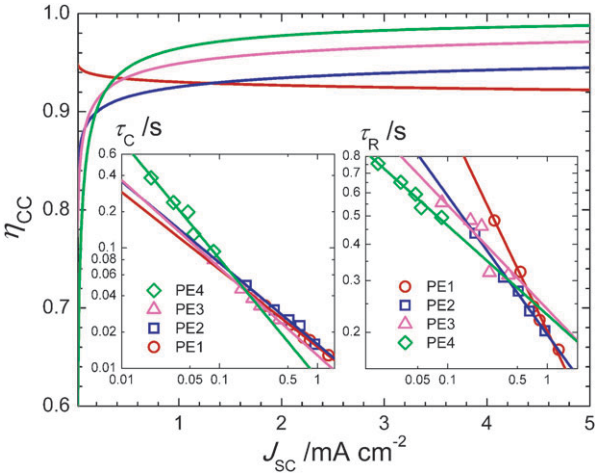

Fig. 5 Efficiency of charge collection (η_{CC}) of NT-DSSC devices of PE1–PE4 as a function of J_{SC} predicted according to $\eta_{CC} = \tau_R/(\tau_C + \tau_R)$. The left and right insets show logarithmic plots of τ_C and τ_R *vs.* J_{SC}, respectively, with the solid lines representing fits of the power-law dependence according to eqn (3).

except PE4 that involves a large experimental uncertainty. The order of curvatures of the TiO_2 potential predicted from τ_C *vs.* J_{SC} is hence PE1 $\geq$ PE2 $\geq$ PE3 > PE4, which is consistent with the results obtained from *C vs.* V_{OC} discussed above.

For the duration τ_R of charge recombination, n was determined to be -0.71 ± 0.06, -0.47 ± 0.04, -0.36 ± 0.18 and -0.31 ± 0.08 for PE1–PE4, respectively, indicating that the variation of τ_R *vs.* J_{SC} is much larger than that of τ_C *vs.* J_{SC}. Furthermore, the order of variation of the former is PE1 > PE2 > PE3 > PE4, which is the reverse of the latter. This observation is contrary to the Ru-dye/TiO_2 nanoparticle (NP) system[10] based on a model of recombination limited by transport, for which the observed change in the diffusion period was equal to the change in the recombination period, *i.e.*, $\tau_R \propto \tau_C$.[10,14] Both τ_R and τ_C increased upon increasing lithium intercalation on TiO_2 NP electrodes; their values have comparable magnitudes. In our case, we used PE1–PE4/TiO_2 NT instead of N719/TiO_2 NP electrodes to fabricate the devices. Our values of τ_R are $\sim$10 times those of τ_C, consistent with the results of a N719/TiO_2 NT system obtained from IMPS/IMVS measurements.[22] The observed larger values of τ_R indicate the superior charge collection characteristic of the NT system relative to the NP system,[22] and the variation of τ_R *vs.* J_{SC} for PE1–PE4 reflects the effect of the length of the link affecting the charge recombination of the system for which a transport-limited model cannot account. The values of τ_R exhibit a systematic trend PE4 > PE3 > PE2 > PE1 at greater J_{SC}, implying that charge recombination can be diminished with a long link under the condition of many injected electrons on TiO_2 films.

Fig. 6 shows a schematic model to rationalize the observed correlations *C vs.* V_{OC}, τ_R *vs.* V_{OC}, τ_C *vs.* J_{SC} and τ_R *vs.* J_{SC} for NT-DSSC devices formed from PE1–PE4. At the left of Fig. 6, we illustrate the conduction band potentials of ATO films adsorbed with a short link (PE1) and a long link (PE4); the potential of the former exceeds that of the latter because of the positive shift of the potential band edge for the system with a long link (Fig. 3). The shift of potential band edge due to dye uptake has not been reported for a conventional

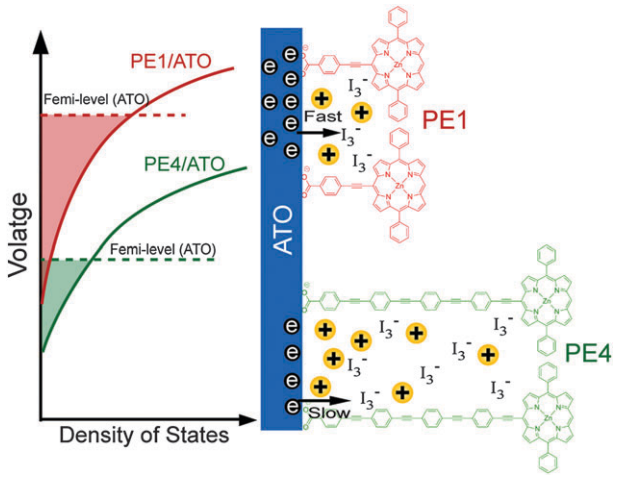

Fig. 6 A model proposed to rationalize the observed correlations of *C vs.* V_{OC}, τ_C *vs.* J_{SC} and τ_R *vs.* J_{SC} for NT-DSSC devices made of porphyrins with varied length of PE link.

DSSC,[5c,d,17–19] but a positive potential shift was due to Li^+ addition[14,15] and the dipole effect in a solid-state DSSC.[16] Porphyrins of this kind might form small aggregated clusters on the surface of semiconductor films.[7] At the right side of Fig. 6 we show a schematic picture to represent the spaces of PE1 and PE4 aggregates (only two of each are presented for clarity) attached on the ATO surface, for which the latter has more room for cations (for instance, Li^+ in the electrolyte)[10,14] to stay near the surface of ATO than the former. As a result, more electrons are expected to be attracted near the ATO surface for PE4 than for PE1, which reasonably accounts for the system with a small potential involving a long link.

We interpret the variations of diffusion and recombination times *vs.* injected electrons under two conditions. With few injected electrons (small J_{SC}), the trap electrons dominate. The PE4 device is expected to have more electrons than the PE1 device trapped on the surface of ATO to interact with cations, so that electrons diffused more slowly for the former than for the latter. We thus expect the duration of diffusion τ_C to decrease from PE4 to PE1 (left inset of Fig. 5) at small J_{SC}. If the trap electrons interact with nearby I_3^- in the electrolyte, we expect the recombination time τ_R measured at an open-circuit condition to increase from PE4 to PE1 (right inset of Fig. 5) at small J_{SC}. In contrast, when many electrons were injected into the conduction band of ATO (large J_{SC}), the electron diffusion would be strongly affected by the shape of the potential. Our results indicate that the short link with a steep potential might have a small rate of diffusion, which leads to the observed τ_C featuring an order PE1 > PE2 > PE3 > PE4 at large J_{SC}. The variation of τ_R exhibits an order the reverse of that of τ_C at large J_{SC} because the charge recombination between detrapped electrons and I_3^- near the porphyrin core is controlled by the length of the link as indicated in the right part of Fig. 6. Therefore, increasing the distance between the redox active center of the sensitizer and the TiO_2 surface effectively decreases the rate of recombination, consistent with the conclusion made elsewhere.[5b–d] The simulated efficiencies of charge collection of PE1–PE4 (Fig. 5) consequently exhibit a systematic trend PE4 > PE3 > PE2 > PE1 at large J_{SC}, demonstrating the advantage of a long link with an improved separation of charge. As porphyrins in this series suffer dye aggregation on TiO_2 films, the efficiencies of electron injection have an order PE1 > PE2 > PE3 > PE4, which predominately determine their cell performances (Fig. 1).

In conclusion, we report the effects of potential shift, electron diffusion and charge recombination on the cell performance for NT-based porphyrin-sensitized solar cells according to our analysis of photocurrent and photovoltage transients. The system with a long link exhibits a positive shift of the TiO_2 potential, consistent with the variation of V_{OC} for PE1–PE4. Both diffusion and recombination times *vs.* J_{SC} are satisfactorily described with a power-law expression and a reverse trend of variation for PE1–PE4, which is rationalized with a model based on the potential shape of TiO_2 and the trap electrons on ATO surface affected by the adsorbed porphyrins with links of varied length. The efficiencies of charge collection of the devices predicted from the simulated τ_C and τ_R values show a systematic trend PE4 > PE3 > PE2 > PE1 at large J_{SC}, implying that a long link improves the charge separation

if the electrons are effectively injected into the semiconductor. This conclusion might assist the design of a new dye/TiO_2 system for DSSC applications.

Acknowledgements

We thank Prof. Juan Bisquert and Dr Arthur Frank for helpful discussions. National Science Council of Taiwan and Ministry of Education of Taiwan, under the ATU program, supported this work.

References

1 (*a*) T. W. Hamann, R. A. Jensen, A. B. F. Martinson, H. V. Ryswyk and J. T. Hupp, *Energy Environ. Sci.*, 2008, **1**, 66; (*b*) M. Grätzel, *Acc. Chem. Res.*, 2009, **42**, 1788; (*c*) H. J. Snaith, *Adv. Funct. Mater.*, 2010, **20**, 13.

2 (*a*) C.-W. Lee, H.-P. Lu, C.-M. Lan, Y.-L. Huang, Y.-R. Liang, W.-N. Yen, Y.-C. Liu, Y.-S. Lin, E. W.-G. Diau and C.-Y. Yeh, *Chem.–Eur. J.*, 2009, **15**, 1403; (*b*) H.-P. Lu, C.-L. Mai, C.-Y. Tsia, S.-J. Hsu, C.-P. Hsieh, C.-L. Chiu, C.-Y. Yeh and E. W.-G. Diau, *Phys. Chem. Chem. Phys.*, 2009, **11**, 10270; (*c*) H.-P. Lu, C.-Y. Tsai, W.-N. Yen, C.-P. Hsieh, C.-W. Lee, C.-Y. Yeh and E. W.-G. Diau, *J. Phys. Chem. C*, 2009, **113**, 20990; (*d*) H. Imahori, T. Umeyama and S. Ito, *Acc. Chem. Res.*, 2009, **42**, 1809.

3 T. Bessho, S. K. Zakeeruddin, C.-Y. Yeh, E. W.-G. Diau and M. Grätzel, *Angew. Chem., Int. Ed.*, 2010, DOI: 10.1002/anie.201002118, in press.

4 (*a*) A. Hagfeldt and M. Grätzel, *Chem. Rev.*, 1995, **95**, 49; (*b*) J. R. Durrant, S. A. Haque and E. Palomares, *Coord. Chem. Rev.*, 2004, **248**, 1247.

5 (*a*) E. Galoppini, *Coord. Chem. Rev.*, 2004, **248**, 1283; (*b*) C. C. Clark, G. J. Meyer, Q. Wei and E. Galoppini, *J. Phys. Chem. B*, 2006, **110**, 11044; (*c*) B. C. O'Regan, I. Lopez-Duarte, M. V. Martinez-Diaz, A. Forneli, J. Albero, A. Morandeira, E. Palomares, T. Torres and J. R. Durrant, *J. Am. Chem. Soc.*, 2008, **130**, 2906; (*d*) A. J. Mozer, P. Wagner, D. L. Officer, G. G. Wallace, W. M. Campbell, M. Miyashita, K. Sunahara and S. Mori, *Chem. Commun.*, 2008, 4741.

6 (*a*) C.-Y. Lin, C.-F. Lo, L. Luo, H.-P. Lu, C.-S. Hung and E. W.-G. Diau, *J. Phys. Chem. C*, 2009, **113**, 755; (*b*) C.-W. Chang, L. Luo, C.-K. Chou, C.-F. Lo, C.-Y. Lin, C.-S. Hung, Y.-P. Lee and E. W.-G. Diau, *J. Phys. Chem. C*, 2009, **113**, 11524.

7 L. Luo, C.-J. Lin, C.-Y. Tsai, H.-P. Wu, L.-L. Li, C.-F. Lo, C.-Y. Lin and E. W.-G. Diau, *Phys. Chem. Chem. Phys.*, 2010, **12**, 1064.

8 M. Myahkostupov, P. Piotrowiak, D. Wang and E. Galoppini, *J. Phys. Chem. C*, 2007, **111**, 2827.

9 C.-C. Chen, H.-W. Chung, C.-H. Chen, H.-P. Lu, C.-M. Lan, S.-F. Chen, L. Luo, C.-S. Hung and E. W.-G. Diau, *J. Phys. Chem. C*, 2008, **112**, 19151.

10 N. Kopidakis, K. D. Benkstein, J. van de Lagemaat and A. J. Frank, *J. Phys. Chem. B*, 2003, **107**, 11307.

11 A. Solbrand, H. Lindström, H. Rensmo, A. Hagfeldt, S.-E. Lindquist and S. J. Södergren, *J. Phys. Chem. B*, 1997, **101**, 2514.

12 B. C. O'Regan, S. Scully, A. C. Mayer, E. Palomares and J. Durrant, *J. Phys. Chem. B*, 2005, **109**, 4616.

13 (*a*) J. Bisquert, *Phys. Chem. Chem. Phys.*, 2003, **5**, 5360; (*b*) J. Bisquert, F. Fabregat-Santiago, I. Mora-Seró, G. Garcia-Belmonte and S. Giménez, *J. Phys. Chem. C*, 2009, **113**, 17278.

14 J. R. Jennings and Q. Wang, *J. Phys. Chem. C*, 2010, **114**, 1715.

15 A. Frank, N. Kopidakis and J. van de Lagemaat, *Coord. Chem. Rev.*, 2004, **248**, 1165.

16 P. Chen, J. H. Yum, F. De Angelis, E. Mosconi, S. Fantacci, S.-J. Moon, R. H. Baker, J. Ko, M. K. Nazeeruddin and M. Grätzel, *Nano Lett.*, 2009, **9**, 2487.

17 M. Miyashita, K. Sunahara, T. Nishikawa, Y. Uemura, N. Koumura, K. Hara, A. Mori, T. Abe, E. Suzuki and S. Mori, *J. Am. Chem. Soc.*, 2008, **130**, 17874.

18 E. M. Barea, R. Caballero, F. Fabregat-Santiago, P. De La Cruz, F. Langa and J. Bisquert, *ChemPhysChem*, 2010, **11**, 245.

19 T. Marinado, K. Nonomura, J. Nissfolk, M. K. Karlsson, D. P. Hagberg, L. Sun, S. Mori and A. Hagfeldt, *Langmuir*, 2010, **26**, 2592.

20 J. Van de Lagemaat, N.-G. Park and A. J. Frank, *J. Phys. Chem. B*, 2000, **104**, 2044.

21 (*a*) J. R. Jennings, A. Ghicov, L. M. Peter, P. Schmuki and A. B. Walker, *J. Am. Chem. Soc.*, 2008, **130**, 13364; (*b*) H. K. Dunn and L. M. Peter, *J. Phys. Chem. C*, 2009, **113**, 4726; (*c*) L. Peter, *Acc. Chem. Res.*, 2009, **42**, 1839.

22 K. Zhu, N. R. Neale, A. Miedaner and A. J. Frank, *Nano Lett.*, 2007, **7**, 69.